Journal of Colloid and Interface Science 491 (2017) 1–12

Contents lists available at ScienceDirect

Journal of Colloid and Interface Science

journal homepage: www.elsevier.com/locate/jcis

Regular Article

Graphene oxide/alginate beads as adsorbents: Influence of the load and the drying method on their physicochemical-mechanical properties and adsorptive performance

Emiliano Platero [a], Maria Emilia Fernandez [a,b], Pablo Ricardo Bonelli [a,b], Ana Lea Cukierman [a,b,c,*]

[a] Universidad de Buenos Aires, Facultad de Ciencias Exactas y Naturales, Departamento de Industrias, Programa de Investigación y Desarrollo de Fuentes Alternativas de Materias Primas y Energía–PINMATE, Intendente Güiraldes 2620, Ciudad Universitaria, (C1428BGA) Buenos Aires, Argentina
[b] Consejo Nacional de Investigaciones Científicas y Técnicas (CONICET), Godoy Cruz 2290, (C1425FQB) Buenos Aires, Argentina
[c] Universidad de Buenos Aires, Facultad de Farmacia y Bioquímica, Departamento de Tecnología Farmacéutica, Cátedra de Farmacotecnia II, Junín 956, (C1113AAD) Buenos Aires, Argentina

GRAPHICAL ABSTRACT

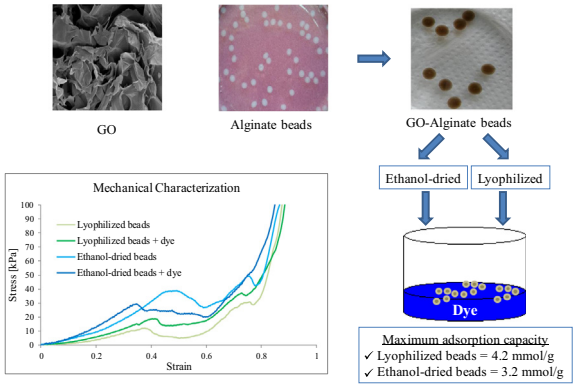

ARTICLE INFO

Article history:
Received 27 September 2016
Revised 7 December 2016
Accepted 9 December 2016
Available online 11 December 2016

Keywords:
Graphene oxide
Alginate beads
Mechanical properties
Basic dye removal

ABSTRACT

Graphene oxide/alginate beads were prepared from lab-synthesized graphene oxide, varying its content within the beads (0.05, 0.125, and 0.25 wt.%). Ethanol-drying and lyophilization were compared as drying methods to obtain suitable adsorbents which were later tested to the removal of a model organic molecule (methylene blue). The morphological and textural properties of all the beads were characterized by scanning electron microscopy and N_2 adsorption/desorption isotherms at −196 °C, respectively. Limited porosity was obtained for all cases (S_{BET} < 60 m^2/g). Uniaxial compression tests were performed to assess the mechanical properties of the beads. Ethanol-dried ones exhibited higher Young's elasticity modulus (E = 192 kPa) than the lyophilized samples (twice at 0.25 wt.% graphene oxide loading), which disclosed breakage points at lower deformation percentages. Adsorption experiments were conducted and dye adsorption isotherms were obtained for the beads with the best removal performance. The experimental data were better fitted by the Langmuir model. The highest maximum adsorption capacity (4.25 mmol/g) was obtained for the lyophilized beads with the highest graphene oxide content. Mechanical properties were found to be affected also by the dye adsorption.

* Corresponding author at: Universidad de Buenos Aires, Facultad de Ciencias Exactas y Naturales, Departamento de Industrias, Programa de Investigación y Desarrollo de Fuentes Alternativas de Materias Primas y Energía–PINMATE, Intendente Güiraldes 2620, Ciudad Universitaria, (C1428BGA) Buenos Aires, Argentina.
E-mail address: analea@di.fcen.uba.ar (A.L. Cukierman).

http://dx.doi.org/10.1016/j.jcis.2016.12.014
0021-9797/

1. Introduction

In the last decade, graphene and related materials have attracted great interest not only in electronic, catalysis and energy but also in environmental applications [1]. In particular, graphene oxide (GO) is a highly oxidized graphene-like structure usually obtained through procedures based on the Hummers' method [2]. GO exhibits the graphene skeleton and a set of oxygen containing functionalities, such as 1,2-epoxides and hydroxyl groups located on the basal planes, and carbonyl, carboxyl and hydroxyl groups at the sheet edges [3]. The adsorption capacity of GO has been tested for heavy metals, synthetic dyes [4] and some other organic compounds, like aniline, nitrobenzene, and chlorobenzene [5]. However, separation of GO from the aqueous media after adsorption tends to be quite difficult because it disperses very well in water; therefore, unpractical high speed centrifugation is usually required [6,7]. To facilitate phase separation of the spent GO many attempts have been made, including functionalization, coupling with magnetic nanoparticles and fabrication of macro-composites with other materials; several reviews have reported on this subject [1,4,8].

Development of composites based on GO and biopolymers could represent an interesting option for the removal of water pollutants. In particular, alginate is a biopolymer that has been employed to obtain 3D macro-composites. It is mainly extracted as sodium alginate from brown seaweed and consists of a linear polysaccharide with homopolymeric blocks of (1,4)-linked β-D-mannuronate and α-L-guluronate. Due to its biodegradability, solubility in water, presence of multiple functional groups and non-toxicity, it has been used not only in the development of adsorbents but also for encapsulation in drug delivery and tissue engineering [9]. Alginate 3D structures can be produced as membranes, hydrogels cylinders or beads depending on the composition of the alginate, the cross-linking agent and the experimental conditions. However, their individual use may suffer from limited stability or weak mechanical resistance. Therefore, stronger hybrid structures have been explored by mixing alginate with other polymers [10,11], clays [12] and, more recently, with nano-carbonaceous materials such as graphene or GO [13,14]. In particular, alginate beads are usually formed by ionic interactions with divalent cations, most commonly Ca^{2+}. Beads composed only by calcium alginate have been used as adsorbents of heavy metals, dyes, and other pollutants [15–17], whereas hybrid alginate beads containing GO within their matrix have only been recently tested in the removal of a few adsorbates, like copper [18], cesium [19] and methylene blue [20].

Most of the works using alginate beads as adsorbents of pollutants usually focus on physicochemical and textural characterization, but very few has dealt with the mechanical properties of the beads. These properties are relevant in order to select the type of equipment and the best operating conditions to achieve good adsorption performance at full-scale. As stated in the literature [21], adsorbents should be able to sustain the load they will be subjected to during handling and adsorption; consequently, an important issue is to determine if deformation affects their use, by reducing the voidage of flattened beads or increasing the resistance of the flow of liquids around them. Mechanical properties of alginate beads have been assessed by measuring the compression strength of single beads by means of uniaxial compression tests [22], and the Hertz theory has been commonly applied to describe the resulting force-deformation curves obtained [23]. Also, from its application, a parameter of stiffness of the beads, given by the Young's modulus (E), can be obtained. The mechanical strength of the beads has been related to alginate composition, in terms of mannuronate/guluronate ratio, and to the type and concentration of the cross-linking divalent cation [24,25]. However, few studies have taken into account the presence of other fillers in the alginate matrix or even how the drying method affects the final characteristics of the beads. The latter is particularly important for their further commercialization as adsorbents. Beads reported in the literature are usually characterized and tested in adsorption assays soon after being produced, and drying is not systematically examined. Moreover, mechanical strength of polymeric beads prior and post adsorption of a pollutant remains almost unexplored. Only recently, Zhang et al. [26] and Jiao et al. [14] studied the compression strength of alginate hydrogel cylinders reinforced with GO, and Chiew et al. [21] showed that Halloysite/alginate beads were mechanically strengthened by both the uptake of Pb^{2+} and the addition of Halloysite nanotubes to the alginate matrix. To the best of our knowledge, no study has yet reported mechanical characterization of GO/alginate beads.

Within this framework, the present work focuses on the development of adsorbents combining GO within an alginate matrix in the form of beads and the characterization of their properties and performance in the removal of a model organic molecule (methylene blue, MB). The effect of the load of GO and the drying method of the beads on the physicochemical and textural characteristics of the developed adsorbents was assessed. Compression tests were performed to analyze the mechanical strength of the beads in terms of the content of GO within the beads and the adsorbed MB. The Hertz's model was subsequently applied to obtain the Young's modulus. The effect of the solution's pH on the adsorption capacities of the beads was examined. Equilibrium adsorption parameters were obtained from the application of mathematical models to experimental adsorption isotherms.

2. Materials and methods

2.1. Materials

Sodium alginate was purchased from Molecule-R®. Commercial graphite, supplied by Serain Juarez S.A., was screen-sieved and the fraction of 37–44 μm mean particle size was selected. Methylene blue (basic blue 9, C.I. 52015, M.W. 373.91 g/mol), purchased from Carlo Erba®, and all the rest of the chemical reagents (H_2SO_4, $KMnO_4$, H_2O_2, $CaCl_2$) were of analytical grade. They were used as received.

2.2. Preparation of GO and the beads

GO was prepared from graphite powder by a modified Hummers' method according to Chen et al. [2,27]. Briefly, concentrated H_2SO_4 was added to 1 g of graphite within a round bottom flask on an ice bath and stirred with a magnetic stirrer. $KMnO_4$ (3 g) was slowly added keeping the temperature below 20 °C. Then, the mixture was vigorously agitated for 30 min at 40 °C. A volume of 50 mL of distilled water was slowly added and the solution was stirred for another 15 min at 95 °C. Additional 150 mL of water were added, followed by 5 mL H_2O_2 (30%) dropwise. The GO dispersion was first centrifuged at 5000 rpm for 5 min to remove the unexfoliated particles and then it was resuspended twice with 1:9 HCl aqueous solution to remove metal ions. Further washing was performed by resuspension in distilled water and centrifugation at 10,000 rpm for 20 min (3 times). To remove any remaining metal or acid contaminant, a dialysis stage (membrane molecular weight cut-off of 12,000–14,000 g/mol, Spectra/Por 5® 12–14 kD) for 2 weeks was added. It was carried out in distilled water within a beaker by constant stirring and regular replacement of the water. Afterwards, the graphite oxide dispersion was sonicated 30 min and stirred for 90 min to exfoliate it to GO nanosheets and finally lyophilized for 48 h (Christ® freeze dryer Alpha 1-4 LD-2). Dried GO was obtained as a compressible sponge.

For the preparation of the beads, a 2% solution of sodium alginate was used. Extrusion dripping method was employed to produce GO/alginate beads with calcium chloride (20 g/L) as the curing agent. GO suspensions of different concentrations were previously added to a volume of the alginate solution (final loads of 0.05; 0.125 and 0.25 wt.% GO) and homogeneously mixed. After formed, the gel beads were kept in the calcium solution with gentle agitation for approximately 2 h. To complete gelation, they were maintained in the solution overnight at 4 °C without agitation. They were subsequently washed several times with distilled water and finally dried either by lyophilization or by a method described by Ma et al. [13]. The latter involves freezing the beads for 12 h at −10 °C, and then immersion in ethanol at room temperature three times, for about 2 h each, and finally dried at 60 °C for 3 h to remove the ethanol. For lyophilization, wet beads were instantly frozen with liquid nitrogen (−196 °C) and then lyophilized for 24 h, with a condenser temperature of −55 °C.

For comparative purposes, alginate beads without GO were also developed and dried by both methods. The ethanol-dried products are hereafter abbreviated as: A for alginate beads, and GOA, GOA2 and GOA3 for alginate beads developed with increasing loads of GO. Similarly, lyophilized ones are abbreviated as AL for alginate beads, and GOAL, GOAL2 and GOAL3 for those containing increasing GO load.

2.3. Characterization of GO and the beads

Elemental composition of GO was assessed by means of an automatic elemental analyzer (Carlo Erba model EA 1108). Ash content in GO was performed according to ASTM standards with a thermal analyzer TA instrument SDT Q-600. This equipment was also employed to investigate the thermal stability of the synthesized GO and the beads; the thermogravimetric analysis was performed in a single heating run at a heating rate of 20 °C/min, under N_2 atmosphere, from room temperature to 600 °C for alginate-containing samples, and to 800 °C for the GO. Capped crucibles were employed to avoid mass loss due to projections of GO debris, as a consequence of the rapid thermal expansion of the material [28].

Identification of surface functionalities on GO, alginate beads and GO/alginate beads was conducted by Fourier Transformed infrared (FT-IR) spectroscopy. The spectra were recorded by transmission method (Nicolet 8700 FTIR Spectrometer) in the range 600–4000 cm^{-1}.

N_2 adsorption-desorption isotherms at −196 °C for the samples were determined with an automatic Micromeritics ASAP-2020 HV volumetric sorption analyzer. Prior to gas adsorption measurements, the dried samples were outgassed at 40 °C overnight. Textural properties were assessed from the isotherms, according to conventional procedures [29]. The Brunauer-Emmett-Teller (BET) surface area (S_{BET}) was determined by the BET procedure, and total pore volume (V_t) was estimated from the amount of N_2 adsorbed at the relative pressure (p/p_0) of 0.99. The volume of micropores (V_μ) was estimated from the cumulative pore volume obtained using the DFT Plus Software (Micromeritics Instrument Corporation), based on the non-local Density Functional Theory, assuming slit pore shape. The mean pore width (W) was calculated from $W = 4\,V_t/S_{BET}$.

Scanning electron microscopy (SEM) was performed in a Zeiss Supra 40 microscope equipped with a field emission gun and coupled with an energy dispersive spectrometer (EDS, Oxford-instrument Inca x-sight). The images were taken with an in-lens detector. To expose the internal features, dried beads were cut with a surgical blade. Whole and cut beads were placed on an aluminum holder, supported on conductive carbon tape and sputter coated with Pt.

The mechanical characteristics of alginate and GO/alginate beads were assessed in terms of stress-strain curves, by uniaxial compression tests carried out with an Instron 3345 Testing Machine. The beads were individually compressed up to 90% of their initial height at a speed of 100 mm/min, at room temperature, after the excess of water was gently eliminated. Six to ten beads from each sample were tested. The beads were selected randomly. Their mean size was determined by means of a caliper. The Hertz theory was applied to describe the experimental data obtained from the compression tests. It relates the applied force (F) and the displacement (H) for a linearly elastic sphere compressed between two rigid surfaces [23]; the analytical solution is given by:

$$F = \frac{4R^{1/2}}{3} E^* \left(\frac{H}{2}\right)^{3/2} \quad (1)$$

where F is the applied force [N], R, the initial radius [m], H, the displacement [m], and E^*, the reduced modulus of the bead [kPa]. The latter can be obtained from the slope of the linear plot of F against $(H)^{3/2}$. In this study, Eq. (1) was applied within the elastic limits of the alginate beads; only data up to 10% strain were used (30% deformation) [9]. The experiments were set at high compression speed to reduce time-dependent behavior of E^*. The Young's modulus (E) can be estimated from:

$$E^* = \frac{E}{1-\upsilon^2} \quad (2)$$

where υ is the Poisson ratio which can be assumed as $\upsilon = 0.5$, considering the beads incompressible (no volume change) at high speed [23].

2.4. Batch experiments

Stock solutions of 2 mmol/L MB were prepared by dissolving the necessary amount of dye in distilled water and diluted to obtain the desired concentrations of the dye. Adsorption experiments were carried out using capped Erlenmeyer flasks in a batch thermostatized system (Lauda Ecoline E200) at 20 ± 0.5 °C, under a wrist-action shaker agitation at a constant speed. After equilibrium was attained and verified, samples were withdrawn and the concentration of the dye in solution was calculated from the measured absorbance at its λ_{max} (663 nm), by means of an UV–Vis spectrophotometer (Shimadzu Model UV mini 1240). The pH effect on the dye adsorption was previously studied in the range 4–9. Dyes solutions were prepared with distilled water and adjusted with HCl and NaOH solutions or maintained with buffers. To compare the performance of the different beads developed, amounts of 0.03 g of the samples were contacted with 50 mL of 0.1 mmol/L MB solution, for 24 h to ensure equilibrium. Dye removal percentages were calculated as follows:

$$Removal\ [\%] = 100\left(\frac{C_o - C_e}{C_o}\right) \quad (3)$$

where C_o and C_e are the initial and equilibrium dye concentrations in solution [mmol/L], respectively.

In addition, equilibrium adsorption isotherms were obtained for the samples of better performance, by contacting 0.03 g of the beads with 50 mL of MB solutions of different initial concentrations (0.05–3.5 mmol/L), until equilibrium was attained. The same temperature and agitation conditions as well as the pH selected were employed. The amount of dye adsorbed per gram of adsorbent at equilibrium, q_e [mmol/g], was calculated as follows:

$$q_e = \frac{(C_o - C_e)V}{m} \quad (4)$$

where C_o is the initial concentration of the dye in the solution [mmol/L], C_e, the equilibrium concentration of dye in the solution

[mmol/L], *V*, the volume of solution [L], and *m*, the mass of beads used [g].

All experiments were performed at least twice. Average values are reported.

3. Results and discussion

3.1. Characterization of GO and the beads

A dried GO sponge was obtained after lyophilization with a light brown color, indicating the successful oxidation of graphite to GO [2]. This material was easily resuspended in water. Preliminary studies showed that with oven-dried GO it was more difficult to achieve a homogenous suspension of the material. The UV–vis absorption spectrum of an aqueous suspension of the obtained GO is shown in Fig. S1 (Supplementary data). It consists of a main absorption peak around 231 nm, usually attributed to π-π^* transition of C=C bonds and a shoulder peak around 300 nm, attributed to n-π^* electronic transition of C=O bonds. This spectrum is in accordance with others reported in literature for GO synthesized through the Hummers' method [2,30].

Table 1 presents the composition of the GO obtained by the elemental analysis. A predominance of C and O was obtained, with a C/O ratio of 1.2. The H content may be related to the presence of the oxygen-containing functional groups. Similar elemental compositions have been reported in the literature [31–33]. Some residual sulfur remained within the obtained GO, as a consequence of the oxidation process, probably in the form of organosulfate and hydroxy sulfate groups [31]. Similar values of S have been reported [34]. The sample, as determined by thermogravimetric analysis, was ash free [35]. The atomic C/O ratio in GO reportedly depends on the graphite used as starting material, the synthesis method and experimental conditions for GO preparation as well as the oxidation degree attained. Results in the literature also show appreciable differences in the reported C/O ratio depending upon the analysis method applied for determination, namely elemental analysis, EDS, XPS. Values of C/O ratios varying between 1 and 3 have been reported [28,33,36]. In this sense, it should be mentioned that the C/O ratio determined in this work by EDS was 1.7 (Table S1 in Supplementary data), a value higher than that obtained by the elemental analysis (1.2). As will be further shown in FT-IR spectra, besides C=C bonds pointing to the aromatic character of GO structure, functional groups such as hydroxyls, carboxyls, sulfates, among others, clearly indicate oxygen presence. In addition, TGA results (shown in Section 3.2) suggest that some of the oxygen determined could come from ambient humidity sorbed during manipulation of the GO sponge [36].

N_2 adsorption/desorption isotherms for the alginate and GO/alginate beads ethanol-dried and lyophilized are illustrated in Fig. 1a and b, respectively. The isotherms obtained for the GO are displayed in Fig. S2 (Supplementary data). The volume of N_2 adsorbed per sample mass unit are represented as a function of the relative pressure (p/p_0), where p is the equilibrium pressure, and p_0, the saturation pressure of the adsorbate at (−196 °C). The

Table 1
Ultimate analysis of the obtained GO.

Ultimate analysis (wt.%)[a]	GO
Carbon	45.2
Hydrogen	1.6
Nitrogen	0.0
Sulfur	1.3
Oxygen[b]	51.9

[a] Dry basis.
[b] Estimated by difference.

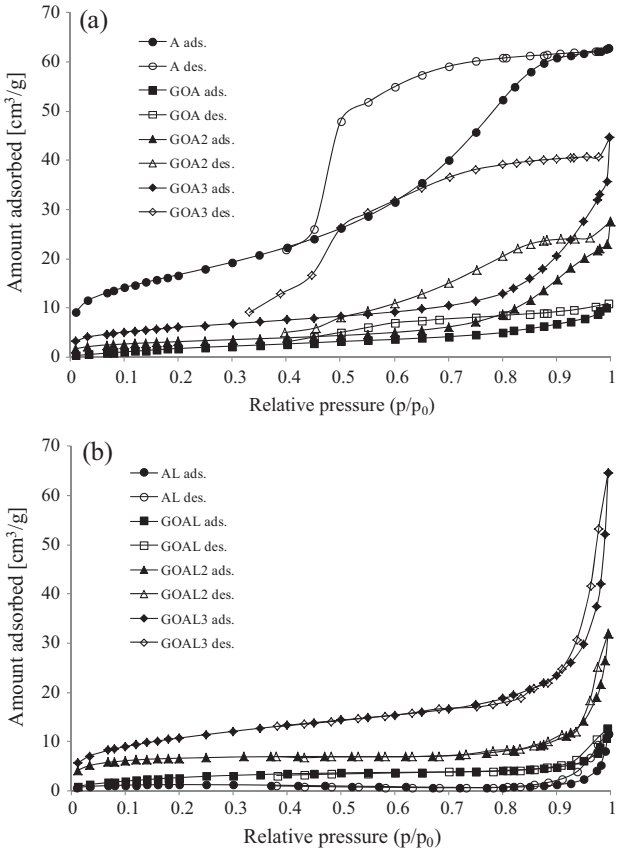

Fig. 1. N_2 adsorption (solid symbols) and desorption (empty symbols) isotherms onto alginate and GO/alginate beads with different GO loading: (a) ethanol-dried and (b) lyophilized.

adsorption isotherm obtained for GO exhibited type I characteristics from the IUPAC classification, with some features of type II too, disclosing the presence of microporous-macroporous structures. Textural parameters of GO and the beads, evaluated from isotherms analysis by the Brunauer-Emmett-Teller (BET) and the DFT methods, are reported in Table 2. The BET surface area and the total pore volume of GO were low compared to predicted theoretical surface area of individual separated graphene sheets (S_{BET} = 2630 m^2/g). However, they were higher than those reported (23–32 m^2/g) for oven-dried synthesized GO [35,37]. The low S_{BET} may be consequence of the re-stacking that occurs when the material is dried, and not in a water suspension, and of the reduction of the separation distance between the sheets [35]. Regarding the beads, the N_2 adsorption/desorption isotherms for ethanol-dried (Fig. 1a) and lyophilized (Fig. 1b) beads displayed visible differences. Comparing beads based only on alginate, the isotherm of A showed clearly a type IV with a pronounced H_2-type hysteresis loop, which is characteristic of mesoporous solids with a broad distribution of pore sizes and shapes and of interconnected pore networks. On the other hand, the ones obtained for AL had type II characteristics, which correspond to macroporous and nonporous adsorbents [38]. As observed from Table 2, AL had much lower surface area and pore development than A. When GO was introduced into the matrices, it may be seen that the increase in GO content within the beads increased the porosity and the S_{BET}, 2.5 times for the ethanol-dried beads and 3.6 times for the lyophilized ones. Similar S_{BET} values have been reported for other GO/alginate composites [13]. Also, the pore widths calculated for the formers were larger, in all cases. Micropores, although present, were very scarce. Similarly to AL, isotherms obtained for GOAL,

Table 2
Textural properties of the obtained GO and the beads.

Sample	S_{BET} (m^2/g)	V_t (cm^3/g)	V_μ (cm^3/g)	W (nm)
GO	166	0.1	0.08	2.4
A	61	0.1	0.04	6.3
GOA	9	0.01	0.007	5.5
GOA2	12	0.03	0.008	10.8
GOA3	22	0.04	0.01	7.7
AL	5	0.004	0.002	3.1
GOAL	11	0.009	0.008	3.4
GOAL2	23	0.02	0.01	3.7
GOAL3	39	0.05	0.02	4.7

GOAL2 and GOAL3 had type II characteristics, with very small desorption hysteresis loops (type H_4), associated to slit-shaped pores. Conversely, GOA, GOA2 and GOA3, also showing type II characteristics, displayed broad hysteresis loops (type H_2), that were more pronounced as GO content increased within the beads. Type H_2 loops are usually associated with complex and not well defined pore structures and with pore mouth smaller than the pore body (ink-bottle geometry) which complicate the pore filling-emptying mechanisms by network effects, pore blocking during evaporation and trapping of adsorbed molecules [39,40].

SEM images of the synthesized GO and the beads are illustrated in Fig. 2a–g, at two different magnifications. Fig. 2a displays the

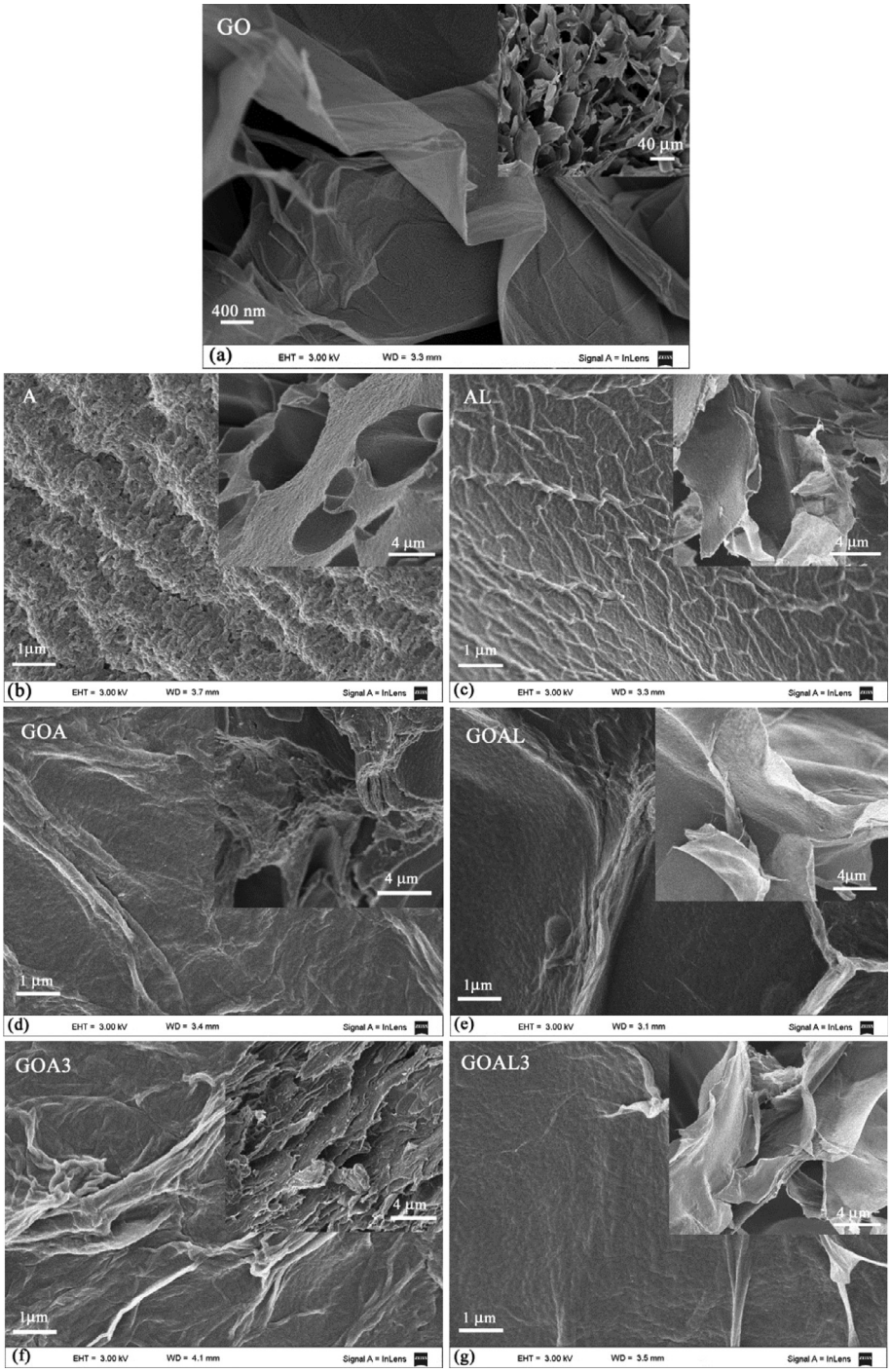

Fig. 2. SEM images of the: (a) obtained GO at 50000× and 2000× (inserted image); (b-g) ethanol-dried and lyophilized beads at 30000× (main image) and 8000× (inserted image) of the alginate beads (b-c), GO (0.05 wt.%)/alginate beads (d-e) and GO (0.25 wt.%)/alginate beads (f-g).

sponge-like structure obtained when drying the GO by lyophilization. The image at the higher magnification shows thin wrinkled sheets with rolled up edges, revealing a crumpled and rippled structure which may be the result of deformations upon the exfoliation and the restacking processes [41]. At lower magnification, the inserted image shows layers of stacked GO, forming not uniformly oriented walls. As previously mentioned, this sponge was easily resuspended in water and combined with the alginate solution to produce the beads. Regarding the beads, Fig. 2b, d and f display the SEM micrographs obtained for ethanol-dried alginate and GO/alginate beads before the adsorption tests. Main images correspond to the beads' outer surface while the image insertions correspond to the inner surface from cut beads. Alginate beads, A, showed a rugged surface (Fig. 2b) with some undulating stripes. This may be related to the higher S_{BET} obtained for this sample (Table 2) in comparison with the rest of the beads. The introduction of GO to the matrix (Fig. 2d and f) seemed to have smoothen the surface and produced some large wrinkles; they were especially noticed at the highest load of GO (Fig. 2f). Inside the beads, A has a macroporous structure with compact and thick walls, while GOA and GOA3 showed more layered walls, due to the addition of GO, which seemed to be oriented mainly in one direction. On the other hand, lyophilized alginate beads, AL, showed the typical network-like outer surface (Fig. 2c), also reported by Kurayama et al. [42]. The small interconnected wrinkles on a more flatten surface differed from the surface of ethanol-dried A sample. In contrast to ethanol-dried samples, the addition of GO (Fig. 2e and g) seemed to smoothen out the outer surfaces, but the larger wrinkles produced were more distant throughout the bead and lesser for GOAL3. The distribution of the internal walls did not changed notoriously with the addition of GO. All samples showed much thinner interconnected walls with large voids. Although it is not appreciated in the micrographs presented here, certain concentricity in the macroporous internal structure was also observed but only for the lyophilized beads. This has also been reported by other authors [43].

In order to identify the main functional groups on the beads, FT-IR spectra were obtained for GO and alginate beads A and AL (Fig. 3a), and GO/alginate beads with the highest GO load, i.e. GOA3 and GOAL3 (Fig. 3b). After the adsorption experiments, later presented in Section 3.5, the spectra for GOA3 and GOAL3 with loaded MB were also obtained; they are also displayed in Fig. 3b. All the spectra show a common broad peak at 3445–3400 cm^{-1}, related to H-bonded —OH groups from carboxyls, phenols and chemisorbed water. Only GO spectrum (Fig. 1a) displayed an absorption peak at 1727 cm^{-1}, attributed to stretching vibrations of

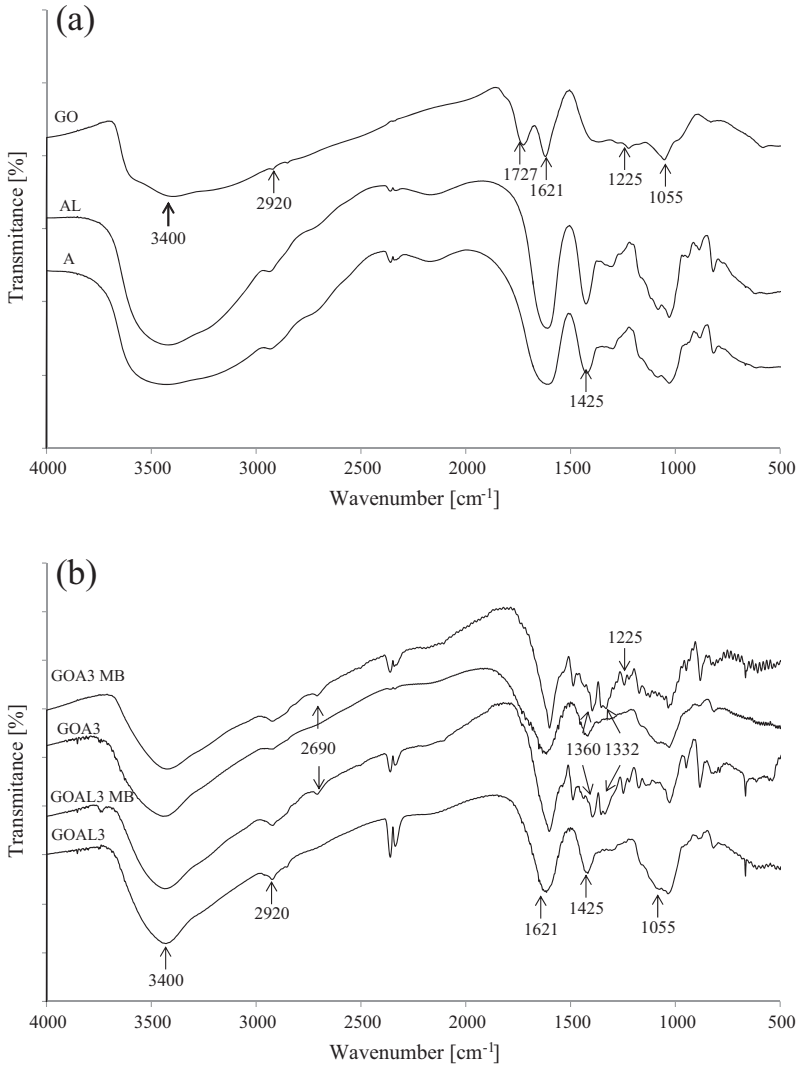

Fig. 3. FT-IR spectra for (a) GO, ethanol-dried and lyophilized alginate beads, (b) ethanol-dried and lyophilized GO/alginate beads with the highest GO load, with and without MB adsorbed.

—C═O in carbonyl groups like esters, ketones and carboxylic acids on the edges and defects of the sheets, indicating an effective oxidation of the graphite. Other peaks at 1225 cm^{-1} and 1055 cm^{-1} were also present, frequently attributed to stretching vibrations of C—C and C—O in epoxides, and a peak at 1621 cm^{-1} which some authors attribute to unoxidized aromatic C═C in GO [44]. Eigler et al. [31] suggest that the peak at 1225 cm^{-1} could also be related to stretching modes of sulfate within GO sheets that overlap with vibrations of epoxy groups. Alginate beads dried by both methods displayed equivalent spectra, suggesting that the drying method did not affect the functional groups present. For the spectra of all the beads (Fig. 3a and b), a small peak was observed at 2920 cm^{-1}, usually assigned to the —CH stretching vibrations of aliphatic —CH_2 and —CH_3 groups. The peak at 1425 cm^{-1}, not observed in GO spectrum, may be assigned to symmetric —COO stretching vibration. Similar spectra were obtained for other GO/alginate beads [18]. On the other hand, the comparison of GOA3 and GOAL3 with and without MB adsorbed may be observed in Fig. 3b. Numerous additional peaks appeared in the spectra obtained for MB loaded beads, i.e. GOA3 MB and GOAL3 MB. In particular, the peak at 2690 cm^{-1} could be assigned to the presence of —$N(CH_3)_2$ terminal saturated groups, while those at 1360 and 1332 cm^{-1} could correspond to C—N and C═S^+ stretching vibrations, all belonging to the MB molecule [45]. Band shifts and reduction of some peaks intensity observed in the spectra of MB-loaded beads confirm the involvement of functional groups of the beads in binding MB molecules to GOA3 and GOAL3. Both π–π stacking interactions and electrostatic interactions have been pointed out as the main adsorption mechanisms for GO/alginate gels [13].

3.2. Thermal stability of GO and the beads

Thermogravimetric analysis (TGA) and differential scanning calorimetry (DSC) of GO, the alginate and GO/alginate beads with three loads of GO and dried by both methods, are illustrated in Fig. 4a–b and c–d, respectively. The thermograms show the mass fraction (m/m_0) as a function of temperature (T), where m and m_0 are the instantaneous and initial mass of the sample. The thermogram for GO (Fig. 4a–b) was consistent with results published by other authors [30,46]. Unlike graphite, whose m/m_0 remained almost unchanged (data not shown), GO underwent a three-step degradation. The sample started to loose mass upon heating below 100 °C, due to evaporation of H_2O and release of carbonaceous gases, such as CO and CO_2, during disproportionation reactions [47], suggesting the presence of structural defects in GO caused by oxidation with a strong acid [48]. A steeper mass loss occurred in the range 180–235 °C, presumably due to the decomposition of labile oxygen-containing functional groups; over 235 °C, the gradual mass loss could be related to more stable functional groups [2]. Regarding the thermograms for the alginate beads A and AL, they had the same shape with a region within 220–320 °C where the mass loss may be ascribed to the breaking of the alginate backbone and loss of the hydroxyl groups of the alginate in the form of water; above 320 °C, the material may decarboxylate and release CO_2 [49]. The rest of the thermograms for the GO/alginate beads had also similar shape.

For samples A, GOA and GOA2, the beginning of the second stage of degradation was shifted to higher temperatures than for GO, around 220 °C. For GOA3, this temperature was closer to that

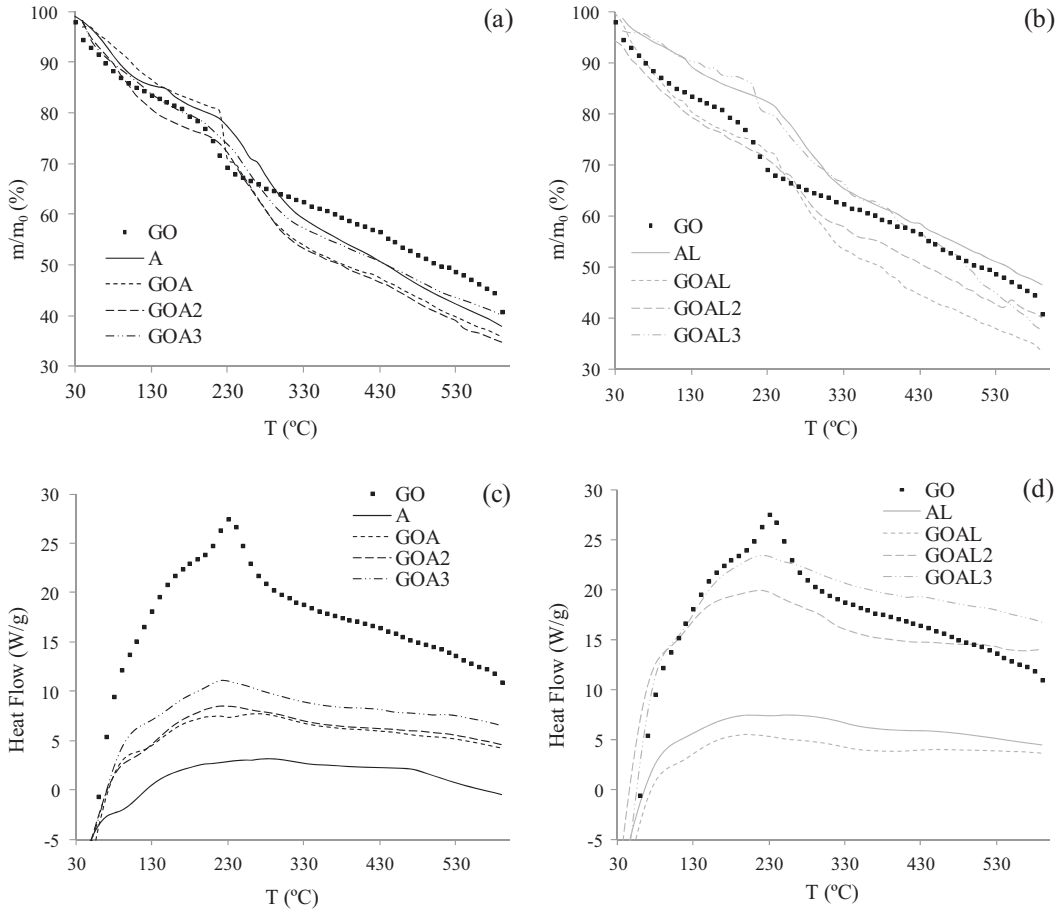

Fig. 4. (a-b) TGA and (c-d) DSC curves for GO, alginate beads and GO/alginate beads.

of GO than to the rest of the beads, starting below 200 °C; this was also observed for the lyophilized GOAL3. This result may be due to the more pronounced effect arising from the highest GO load. It has also been attributed to the enhanced thermal conductivity of GO aiding bond cleavage at the highest load of the nanomaterial [18]. The thermal conductivity and the cleavage of oxygen containing groups, some of which could be involved in the linking to the backbone of alginate, might promote the rupture of this backbone and the release of these groups from the matrix at lower temperatures than those for beads without GO sheets. Interestingly, GOA had an unusual mass loss of about 10% in the range 220–225 °C. A similar behavior was also observed for the lyophilized beads of GOAL3 but with a smaller drop, of around 5%. Evidence of interactions between GO and alginate have been reported in the literature [14,26,48], suggesting crosslinking between the edges of GO sheets and alginate chains through hydrogen bonds. The crosslinking of high loads of GO within the alginate matrix might cause a mild decrease in the thermal stability of these beads in comparison to plain alginate beads, as the temperature at which the second stage of degradation started was lower. Lower thermal stability of GO/polymer composites was also reported by Yadav et al. [48]. From DSC curves (Fig. 4c–d) it can be observed a well defined peak at 230 °C for the GO sample, corresponding to its exothermic decomposition [50]. In the case of the beads without or with low amount of GO loaded, no distinctive peak could be observed, whereas curves for samples GOA3 and GOAL3 showed a small peak but with a slight shift of the maximum, to 220 °C, probably indicating some interactions between the polymer and GO.

3.3. Effect of the GO load and the drying method on the size of the beads

All the beads obtained, before drying, were quite spherical, with reasonably uniform size. Once dried, the lyophilized beads maintained this shape, while the ethanol-dried ones crushed into a more pelletized form. Dried AL was smaller in size than the beads with the added GO. The filler may have acted as structural support, helping to maintain the shape and preventing collapse and shrinkage during lyophilization [43]. In all cases, once in contact with aqueous solutions, both types of beads regained the spherical shape. The sizes of the wet alginate beads were examined with regard to the presence or absence of GO and of the dye adsorbed. Fig. 5a and b depict the mean size of wet alginate and GO/alginate beads, ethanol-dried (Fig. 5a) and lyophilized (Fig. 5b), as well as obtained after the MB adsorption experiments, whether from the dye's solution or from the blanks, i.e. without the dye. From these figures, it can be inferred that the incorporation of GO affected the size of the beads. There is a clear tendency of reduced swelling of the beads in solution with increasing GO content within the beads; although this was observed for both ethanol-dried and lyophilized beads, the effect was more pronounced for the former ones. It should also be noted that the mean size of alginate beads, A and AL, in relation to the beads produced with the smallest load of GO, GOA and GOAL, did not differ significantly in size, in agreement with those obtained after the adsorption of the dye. This suggests that there is a minimum load of GO which starts altering the size and the morphological structure (Fig. 2) of the beads, although textural parameters of ethanol-dried beads changed with the very first incorporation of GO (Table 2).

Additionally, after the adsorption of MB, the beads showed smaller sizes compared to the blank beads. This tendency was observed for both the ethanol-dried and the lyophilized samples. There was a reduced swelling when the dye was also present in the solution. A similar phenomenon was also reported by Mohammed et al. [51] who attributed it to a less polar environment within the gel beads as the MB accumulates and increases the hydrophobicity, producing more compact structures. Only GOA3 did not significantly changed their size after the adsorption of the dye.

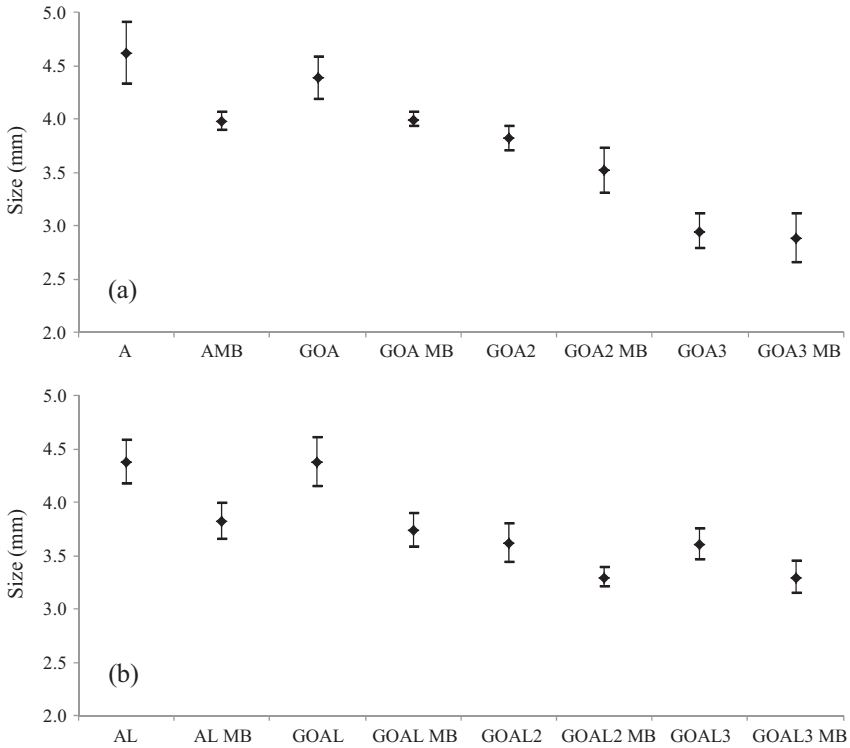

Fig. 5. Mean size of alginate and GO/alginate beads (a) ethanol-dried and (b) lyophilized, with and without MB adsorbed.

3.4. Effect of the GO load and the drying method on the mechanical properties of the beads

The mechanical behavior of the beads was evaluated from compression tests performed on wet alginate and GO/alginate beads obtained after the MB adsorption experiments, whether from the dye's solution or from the blanks. During compression, the normal force was measured at a given deformation, from which stress-strain curves were obtained. Representative curves are presented in Fig. 6a–d. The ethanol-dried beads (Fig. 6a) seemed to be more elastic even after deformation at 40% strain, while the lyophilized beads (Fig. 6b) disclosed breakage points at lower stress and lower deformation percentage. Likewise, as the GO load increased, the beads became more brittle and cracked at lower strains. According to Chan et al. [43], the increase in the load led to fewer voids and denser packing; therefore, the beads lose certain flexibility, as they become more brittle. When comparing with beads which have adsorbed MB (Fig. 6c and d), the cracking at even lower strains is well observed, especially for samples GOA3 MB and GOAL3 MB, with the highest GO load.

In order to relate the mechanical properties of the beads and their structure, the Young's modulus (E) was determined for each sample. Fig. 7a and b illustrate the mean Young's moduli, calculated as depicted in Section 2.3, for ethanol-dried and lyophilized beads, respectively, within the elastic limits of the alginate beads (up to 10% strain). First, it can be observed that the E value increased with the addition of GO to the beads, pointing to a stiffening effect. This has also been reported for chitosan/graphene composites [52] and glycerol-plasticized starch/GO [44]. The improvement of this mechanical property of the beads has been attributed to electrostatic interactions between the reinforcing material and the polymer matrices [52] and a fine dispersion of the GO sheets within the polymers [53].

It was also noticed that the E values obtained for the beads tested in this work were below some of the values reported for other alginate beads [9,25]. Additionally to factors like the natural variability of the alginate from the seaweed source, the size of the beads and the experimental conditions to obtain them, this result may be related to the fact that the beads are tested after rehydration and not as soon as they are produced, i.e. before being dried. Then, the drying itself could have weakened the beads' structure. Comparing the two drying methods, the E values for the ethanol-dried beads were somewhat higher than for the lyophilized ones; indeed, this was particularly evident for GOA3 and GOAL3. Lyophilization may have caused the structure of the beads to debilitate when water sublimated from the matrix [43]. It is also worth noting that the accumulation of the dye inside the beads conferred them further rigidity; this was observed for the beads with the two lower loads of GO (0.05 and 0.125 wt.%). The Young's moduli for GOA3 and GOAL3 did not noticeably change with the adsorption of MB. A greater dispersion of the E values was also noted for these samples.

3.5. Dye adsorption onto the beads

Preliminary adsorption tests were run to asses the stability of the beads at different pH and, at the same time, to determine at which solution's pH the highest dye removal was achieved. From these tests, it was observed that at pH 9 the beads partially degraded. Besides, at pH 4, although integrity was not an issue, the maximum removal achieved was about 10% lower than at pH 7; therefore, neutral pH was chosen as the optimum value to run the experiments. Fig. 8 compares the adsorption performance of all beads produced at a given dose and dye solution concentration. Clearly, the increase in GO content led to a rise in the dye removal by both ethanol-dried and lyophilized beads, in similar percentages. At least a 30% improvement in the performance of MB adsorption was achieved with the beads with the highest GO load, GOA3 and GOAL3. Despite presenting the highest S_{BET} (Table 2), sample A, without GO, had the lowest removal percentage. The increment of GO nanosheets within the GO/alginate beads led to increasing porosity (Table 2) and accessibility, possibly resulting in the improved adsorption of MB, as the dye interacts not only with the alginate structure but also with the GO nanosheets.

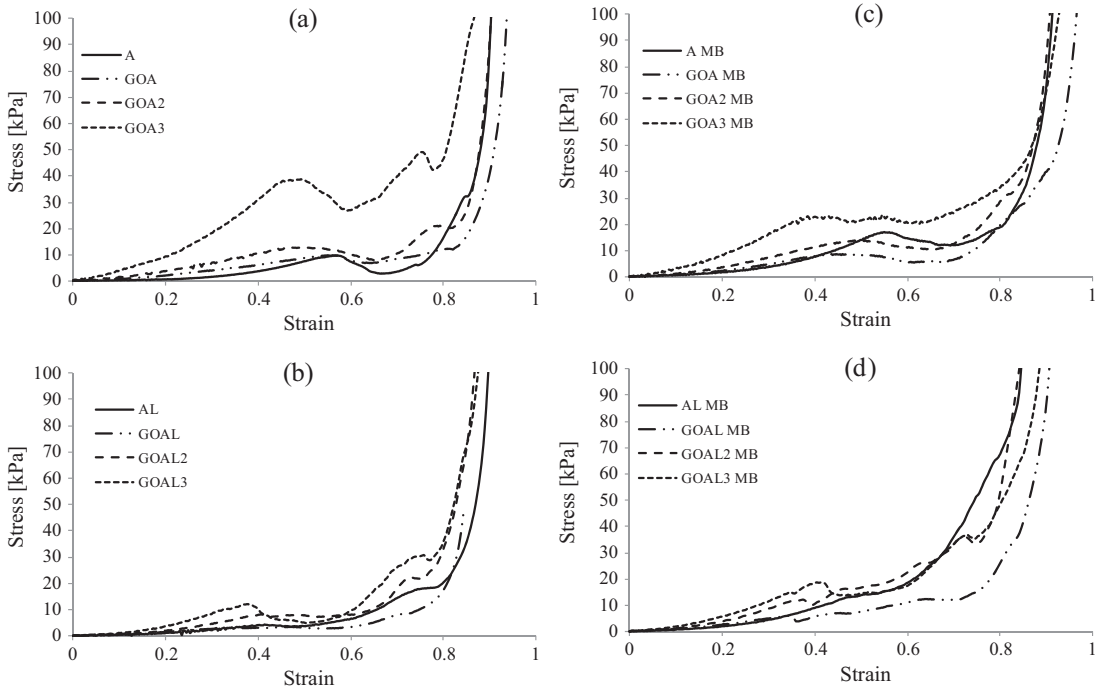

Fig. 6. Stress-strain curves for alginate and GO/alginate beads (a) ethanol-dried and (b) lyophilized without MB adsorbed and (c-d) with MB adsorbed, respectively.

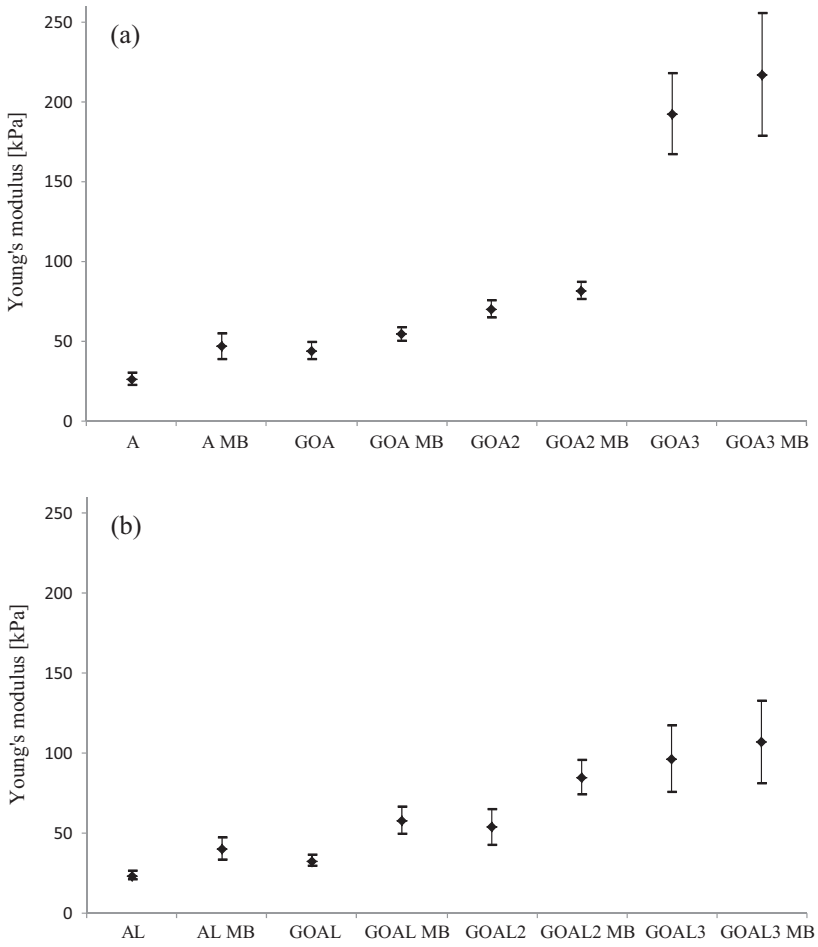

Fig. 7. Young's modulus for alginate and GO/alginate beads (a) ethanol-dried and (b) lyophilized, with and without MB adsorbed.

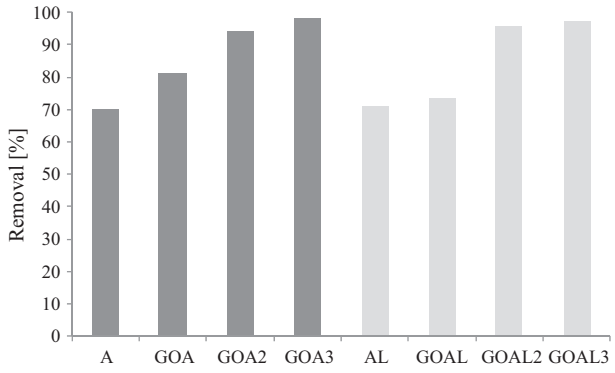

Fig. 8. Effect of the incorporation of GO to the ethanol-dried and lyophilized alginate beads on the adsorption of methylene blue (MB) at equilibrium. C_0 = 0.1 mmol/L, dose: 0.03 g/50 mL, pH = 7.

According to Ma et al. [13], besides the interaction between the carboxyl groups of alginate and MB, electrostatic interaction would be the main binding strength between the oxygen containing groups of GO and MB.

Based on the results shown in Fig. 8, GOA3 and GOAL3 were selected as the best adsorbents and their corresponding adsorption isotherms for MB were obtained. They are presented in Fig. 9a and b, respectively. Two common adsorption models were comparatively applied for experimental data fitting. The Langmuir model, described by the following equation:

$$q_e = \frac{k_L q_{mL} C_e}{1 + k_L C_e} \tag{5}$$

where q_e is the amount of MB adsorbed at equilibrium per unit mass of adsorbent [mmol/g], k_L, the Langmuir constant [L/mmol], q_{mL}, the maximum amount adsorbed corresponding to complete monolayer surface coverage [mmol/g] and C_e, the equilibrium concentration of the adsorbate in solution [mmol/L]. Also, the Freundlich model was applied, represented by:

$$q_e = k_F C_e^{n_F} \tag{6}$$

where k_F [(mmol/g)(L/mmol)$^{n}_{F}$] and n_F are the Freundlich isotherm constants related to adsorption capacity and intensity, respectively. Models predictions are also illustrated in Fig. 9a and b and estimated model parameters are listed in Table 3. The experimental isotherms (Fig. 9a and b) were concave and showed a saturation trend at high dye concentrations. The Langmuir model fitted data very well ($r^2 > 0.98$), suggesting monolayer coverage with the dye and equivalent adsorption sites for both adsorbents. The Freundlich model exhibited a less appropriate fit. The adsorption of MB seemed to be more intense in GOA3, as inferred from the k_L values, almost twice higher for this adsorbent. However, the highest maximum adsorption capacity (q_{mL}) was obtained with GOAL3 as adsorbent. Since apart from the drying method there were no other differences in the adsorbents' preparation, it could be inferred that the drying method was crucial for this result. Both adsorption capacities for MB are comparable to the highest values listed in the recent review by Cukierman et al. for adsorbents developed with graphene and GO

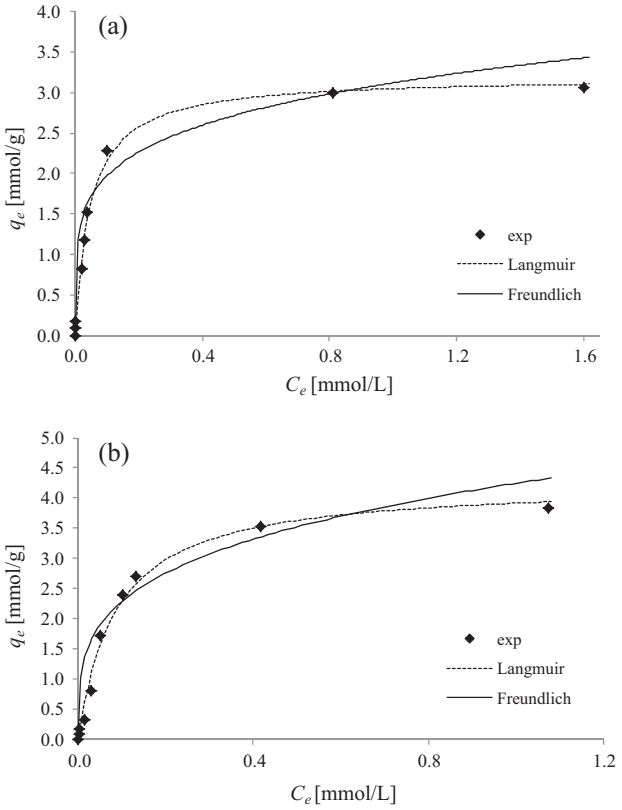

Fig. 9. Equilibrium adsorption isotherms for methylene blue (MB) onto (a) GOA3 and (b) GOAL3. Comparison between the experimental data (points) and predictions of the Langmuir and Freundlich models (lines). Dose: 0.03 g/50 mL, pH = 7.

Table 3
Model parameters estimated for the adsorption isotherms of methylene blue (MB) onto GOA3 and GOAL3.

Model		GOA3	GOAL3
Langmuir	q_{mL} (mmol/g)	3.2	4.2
	k_L (L/mmol)	20.6	11.7
	r^2	0.994	0.988
Freundlich	n_F	0.20	0.27
	k_F ((mmol/g)(L/mmol)^{nF})	3.1	4.2
	r^2	0.846	0.826

[8] and superior to those listed in reviews for conventional adsorbents, including commercial activated carbons [54,55].

4. Conclusions

GO/alginate beads with different loading of lab-synthesized GO were obtained and successfully tested as adsorbents of methylene blue, used as a representative model organic molecule. The almost unexplored effect of the drying method, namely ethanol-drying or lyophilization, on physicochemical-mechanical characteristics of the resulting beads and on their adsorption performance was systematically examined. This aspect has been almost unexplored previously in the literature. The drying method was found to especially affect the morphology and porous characteristics of the resulting beads, with those obtained by lyophilization exhibiting a relatively more pronounced porous development. The latter was also favored by increasing GO load, as reflected in higher values of the BET surface area and total pore volume. Instead, neither the functional groups present nor the thermal behavior of the beads were particularly altered by the drying method. Special emphasis was placed on the mechanical properties of the beads. Interestingly, these properties, scarcely examined in the literature for similar hybrid nanostructured materials, were found to be affected not only by the drying method and the load of GO, but also by the adsorption of the dye itself. The ethanol-dried beads were found to be more elastic compared to the lyophilized ones. Both GO load and the dye adsorbed increased the Young's moduli of the beads, suggesting that they became more stiffened. Furthermore, differences in the maximum adsorption capacities of the beads, depending on the drying method, were determined. The lyophilized GO/alginate beads with the highest GO load showed a 30% higher adsorption capacity than those obtained by ethanol drying, and also superior to those reported for other nanocomposites and activated carbons including developed and commercial samples.

Overall, present results may contribute to the development of a new generation of adsorbents based on GO nano-sheets and consequently, to attain sustainable, more efficient technologies for full-scale effluents treatment. Nevertheless, more research is still needed to achieve this goal. In this direction, future work should be extended towards the improvement of mechanical properties of the nanoadsorbents as well as adsorption studies involving multicomponent solutions and/or real complex effluents under dynamic conditions for a closer approach to real conditions, in order to accomplish reliable information for the proper design and operation of large-scale adsorption units.

Acknowledgements

The authors gratefully acknowledge Consejo Nacional de Investigaciones Científicas y Técnicas (CONICET) [PIP11220090100183], Fondo para la Investigación Científica y Tecnológica-Agencia Nacional de Promoción Científica y Tecnológica (FONCYT-ANPCYT) [PICT 2012-0183] and Universidad de Buenos Aires (UBA) [UBACYT 20020130100605BA] from Argentina, for its financial support.

Appendix A. Supplementary material

Supplementary data associated with this article can be found, in the online version, at http://dx.doi.org/10.1016/j.jcis.2016.12.014.

References

[1] C. Li, G. Shi, Three-dimensional graphene architectures, Nanoscale 4 (2012) 5549–5563.
[2] J. Chen, Y. Li, L. Huang, C. Li, G. Shi, High-yield preparation of graphene oxide from small graphite flakes via an improved Hummers method with a simple purification process, Carbon 81 (2015) 826–834.
[3] J. Guerrero-Contreras, F. Caballero-Briones, Graphene oxide powders with different oxidation degree, prepared by synthesis variations of the Hummers method, Mater. Chem. Phys. 153 (2015) 209–220.
[4] S. Chowdhury, R. Balasubramanian, Recent advances in the use of graphene-family nanoadsorbents for removal of toxic pollutants from wastewater, Adv. Colloid. Interfac. 204 (2014) 35–56.
[5] H. Yan, H. Wu, K. Li, Y. Wang, X. Tao, H. Yang, R. Cheng, Influence of the surface structure of graphene oxide on the adsorption of aromatic organic compounds from water, ACS Appl. Mater. Interf. 7 (2015) 6690–6697.
[6] B. Yu, J. Xu, J.H. Liu, S.T. Yang, J. Luo, Q. Zhou, J. Wan, R. Liao, H. Wang, Y. Liu, Adsorption behavior of copper ions on graphene oxide–chitosan aerogel, J. Environ. Chem. Eng. 1 (2013) 1044–1050.
[7] X. Li, X. Tang, Y. Fang, Using graphene oxide as a superior adsorbent for the highly efficient immobilization of Cu(II) from aqueous solution, J. Mol. Liq. 199 (2014) 237–243.
[8] A.L. Cukierman, E. Platero, M.E. Fernandez, P.R. Bonelli, Potentialities of graphene-based nanomaterials for wastewater treatment, in: A.K. Mishra (Ed.), Smart Materials for Waste Water Applications, Wiley-Scrivener Publishing LLC, MA, United States, 2016, pp. 47–86.
[9] C.S.C. Chiew, P.E. Poh, P. Pasbakhsh, B.T. Tey, H.K. Yeoh, E.S. Chan, Physicochemical characterization of halloysite/alginate bionanocomposite hydrogel, Appl. Clay. Sci. 101 (2014) 444–454.

[10] K. Zhang, Y. Xu, X. Hua, H. Han, J. Wang, J. Wang, Y. Liu, Z. Liu, An intensified degradation of phenanthrene with macroporous alginate–lignin beads immobilized *Phanerochaete chrysosporium*, Biochem. Eng. J. 41 (2008) 251–257.
[11] B. Hui, Y. Zhang, L. Ye, Preparation of PVA hydrogel beads and adsorption mechanism for advanced phosphate removal, Chem. Eng. J. 235 (2014) 207–214.
[12] M. Ghadiri, W. Chrzanowski, W.H. Lee, A. Fathi, F. Dehghani, R. Rohanizadeh, Physico-chemical, mechanical and cytotoxicity characterizations of Laponite®/alginate nanocomposite, Appl. Clay. Sci. 85 (2013) 64–73.
[13] T. Ma, P.R. Chang, P. Zheng, F. Zhao, X. Ma, Fabrication of ultra-light graphene-based gels and their adsorption of methylene blue, Chem. Eng. J. 240 (2014) 595–600.
[14] C. Jiao, J. Xiong, J. Tao, S. Xu, D. Zhang, H. Lin, Y. Chen, Sodium alginate/graphene oxide aerogel with enhanced strength–toughness and its heavy metal adsorption study, Int. J. Biol. Macromol. 83 (2016) 133–141.
[15] R. Aravindhan, N.N. Fathima, J.R. Rao, B.U. Nair, Equilibrium and thermodynamic studies on the removal of basic black dye using calcium alginate beads, Colloid. Surface. A 299 (2007) 232–238.
[16] S. Peretz, O. Cintez, Removal of some nitrophenol contaminants using alginate gel beads, Colloid. Surface. A 319 (2008) 165–172.
[17] T. Lu, T. Xiang, X.L. Huang, C. Li, W.F. Zhao, Q. Zhang, C.S. Zhao, Post-crosslinking towards stimuli-responsive sodium alginate beads for the removal of dye and heavy metals, Carbohyd. Polym. 133 (2015) 587–595.
[18] W.M. Algothmi, N.M. Bandaru, Y. Yu, J.G. Shapter, A.V. Ellis, Alginate-graphene oxide hybrid gel beads: an efficient copper adsorbent material, J. Colloid. Interf. Sci. 397 (2013) 32–38.
[19] H. Yang, H. Li, J. Zhai, L. Sun, Y. Zhao, H. Yu, Magnetic prussian blue/graphene oxide nanocomposites caged in calcium alginate microbeads for elimination of cesium ions from water and soil, Chem. Eng. J. 246 (2014) 10–19.
[20] Y. Zhuang, F. Yu, J. Chen, J. Ma, Batch and column adsorption of methylene blue by graphene/alginate nanocomposite: comparison of single-network and double-network hydrogels, J. Environ. Chem. Eng. 4 (2016) 147–156.
[21] C.S.C. Chiew, H.K. Yeoh, P. Pasbakhsh, K. Krishnaiah, P.E. Poh, B.T. Tey, E.S. Chan, Halloysite/alginate nanocomposite beads: kinetics, equilibrium and mechanism for lead adsorption, Appl. Clay. Sci. 119 (2016) 301–310.
[22] S.V. Bhujbal, G.A. Paredes-Juarez, S.P. Niclou, P. De Vos, Factors influencing the mechanical stability of alginate beads applicable for immunoisolation of mammalian cells, J. Mech. Behav. Biomed. Mater. 37 (2014) 196–208.
[23] C.X. Wang, C. Cowen, Z. Zhang, C.R. Thomas, High-speed compression of single alginate microspheres, Chem. Eng. Sci. 60 (2005) 6649–6657.
[24] C. Ouwerx, N. Velings, M.M. Mestdagh, M.A.V. Axel, Physico-chemical properties and rheology of alginate gel beads formed with various divalent cations, Polym. Gels Netw. 6 (1998) 393–408.
[25] E.S. Chan, T.K. Limb, W.P. Voo, R. Pogaku, B.T. Tey, Z. Zhang, Effect of formulation of alginate beads on their mechanical behavior and stiffness, Particuology 9 (2011) 228–234.
[26] H. Zhang, X. Pang, Y. Qi, PH-Sensitive graphene oxide/sodium alginate/polyacrylamide nanocomposite semi-IPN hydrogel with improved mechanical strength, RSC Adv. 5 (2015) 89083–89091.
[27] W.S. Hummers, R.E. Offeman, Preparation of graphitic oxide, J. Am. Chem. Soc 80 (1958) 1339.
[28] S. Stankovich, D.A. Dikin, R.D. Piner, K.A. Kohlhaas, A. Kleinhammes, Y. Jia, Y. Wu, S.B.T. Nguyen, R.S. Ruoff, Synthesis of graphene-based nanosheets via chemical reduction of exfoliated graphite oxide, Carbon 45 (2007) 1558–1565.
[29] M.E. Fernandez, G.V. Nunell, P.R. Bonelli, A.L. Cukierman, Activated carbon developed from orange peels: batch and dynamic competitive adsorption of basic dyes, Ind. Crop. Prod. 62 (2014) 437–445.
[30] V. Panwar, A. Chattree, K. Pal, A new facile route for synthesizing of graphene oxide using mixture of sulfuric–nitric–phosphoric acids as intercalating agent, Physica E 73 (2015) 235–241.
[31] S. Eigler, C. Dotzer, F. Hof, W. Bauer, A. Hirsch, Sulfur species in graphene oxide, Chem. Eur. J. 19 (2013) 9490–9496.
[32] J. Song, X. Wang, C.T. Chang, Preparation and characterization of graphene oxide, J. Nanomater. 2014 (2014) 1–6.
[33] C. Botas, P. Álvarez, C. Blanco, R. Santamaría, M. Granda, P. Ares, F. Rodríguez-Reinoso, R. Menéndez, The effect of the parent graphite on the structure of graphene oxide, Carbon 50 (2012) 275–282.
[34] A. Dimiev, D.V. Kosynkin, L.B. Alemandy, P. Chaguine, J.M. Tour, Pristine graphite oxide, J. Am. Chem. Soc. 134 (2012) 2815–2822.
[35] R.S. Ribeiro, A.M.T. Silva, L.M. Pastrana-Martínez, J.L. Figueiredo, J.L. Faria, H.T. Gomes, Graphene-based materials for the catalytic wet peroxide oxidation of highly concentrated 4-nitrophenol solutions, Catal. Today 249 (2015) 204–212.
[36] C. Petit, M. Seredych, T. Bandosz, Revisiting the chemistry of graphite oxides and its effect on ammonia adsorption, J. Mater. Chem. 19 (2009) 9176–9185.
[37] Y. Li, Q. Du, T. Liu, X. Peng, J. Wang, J. Sun, Y. Wang, S. Wu, Z. Wang, Y. Xia, L. Xia, Comparative study of methylene blue dye adsorption onto activated carbon, graphene oxide, and carbon nanotubes, Chem. Eng. Res. Des. 91 (2013) 361–368.
[38] C. Sangwichien, G.L. Aranovich, M.D. Donohue, Density functional theory predictions of adsorption isotherms with hysteresis loops, Colloid. Surface. A 206 (2002) 313–320.
[39] K.S.W. Sing, Physisorption of gases by porous carbons, in: J.W. Patrick (Ed.), Porosity in Carbons: Characterization and Applications, Halsted Press, Wiley & Sons Inc., New York, 1995, pp. 49–66.
[40] A. Tarafdar, S. Biswas, N.K. Pramanik, P. Pramanik, Synthesis of mesoporous chromium phosphate through an unconventional sol–gel route, Micropor. Mesopor. Mat. 89 (2006) 204–208.
[41] C. Fu, G. Zhao, H. Zhang, S. Li, Evaluation and characterization of reduced graphene oxide nanosheets as anode materials for lithium-ion batteries, Int. J. Electrochem. Sci. 8 (2013) 6269–6280.
[42] F. Kurayama, S. Suzuki, T. Oyamada, T. Furusawa, M. Sato, N. Suzuki, Facile method for preparing organic/inorganic hybrid capsules using amino-functional silane coupling agent in aqueous media, J. Colloid- Interf. Sci. 349 (2010) 70–76.
[43] E.S. Chan, S.L. Wong, P.P. Lee, J.S. Lee, T.B. Ti, Z. Zhang, D. Poncelet, P. Ravindra, S.H. Phan, Z.H. Yim, Effects of starch filler on the physical properties of lyophilized calcium–alginate beads and the viability of encapsulated cells, Carbohyd. Polym. 83 (2011) 225–232.
[44] W.H. Ferreira, C.T. Andrade, Characterization of glycerol-plasticized starch and graphene oxide extruded hybrids, Ind. Crop. Prod. 77 (2015) 684–690.
[45] O.V. Ovchinnikov, A.V. Evtukhova, T.S. Kondratenko, M.S. Smirnov, V.Y. Khokhlov, O.V. Erina, Manifestation of intermolecular interactions in FTIR spectra of methylene blue molecules, Vibr. Spectrosc. 86 (2016) 181–189.
[46] C.R. Arza, P. Jannasch, F.H.J. Maurer, Network formation of graphene oxide in poly (3-hydroxybutyrate) nanocomposites, Eur. Polym. J. 59 (2014) 262–269.
[47] K. Raidongia, A.T.L. Tan, J. Huang, Graphene oxide: some new insights into an old material, in: K. Tanaka, S. Iijima (Eds.), Carbon Nanotubes and Graphene, Elsevier Ltd., Amsterdam, 2014, pp. 341–374.
[48] M. Yadav, K.Y. Rhee, S.J. Park, Synthesis and characterization of graphene oxide/carboxymethylcellulose/alginate composite blend films, Carbohyd. Polym. 110 (2014) 18–25.
[49] B. Kusuktham, J. Prasertgul, P. Srinun, Morphology and property of calcium silicate encapsulated with alginate beads, Silicon 6 (2014) 191–197.
[50] Y. Qiu, F. Guo, R. Hurt, I. Külaots, Explosive thermal reduction of graphene oxide-based materials: mechanism and safety implications, Carbon 72 (2014) 215–223.
[51] N. Mohammed, N. Grishkewich, H.A. Waeijen, R.M. Berry, K.C. Tam, Continuous flow adsorption of methylene blue by cellulose nanocrystal-alginate hydrogel beads in fixed bed columns, Carbohyd. Polym. 136 (2016) 1194–1202.
[52] A.M. Pandele, M. Ioniță, H. Iovu, Molecular modeling of mechanical properties of the chitosan based graphene composites, U.P.B. Sci. Bull. Series B 76 (1) (2014) 107–112.
[53] T. Kuilla, S. Bhadra, D. Yao, N.H. Kim, S. Bose, J.H. Lee, Recent advances in graphene based polymer composites, Prog. Polym. Sci. 35 (2010) 1350–1375.
[54] G. Mezohegyi, F.P. van der Zee, J. Font, A. Fortuny, A. Fabregat, Towards advanced aqueous dye removal processes: a short review on the versatile role of activated carbon, J. Environ. Manage. 102 (2012) 148–164.
[55] M.J. Ahmed, Application of agricultural based activated carbons by microwave and conventional activations for basic dye adsorption: review, J. Environ. Chem. Eng. 4 (2016) 89–99.